

Local atomic structure of α -Pu

F. J. Espinosa, P. Vilella, J. C. Lashley, and S. D. Conradson

Materials Science and Technology Division, Los Alamos National Laboratory, Los Alamos, New Mexico 87545

L. E. Cox, R. Martinez, B. Martinez, L. Morales, J. Terry, and R. A. Pereyra

Nuclear Materials Technology Division, Los Alamos National Laboratory, Los Alamos, New Mexico 87545

(Received 20 November 2000; published 16 April 2001)

The local atomic structure of α -Pu was investigated using x-ray absorption fine structure (XAFS) spectroscopy. XAFS spectra were obtained for a zone-refined α -Pu and the results were compared to 32-year-old and Ce-doped (0.34 at. %) samples. X-ray diffraction (XRD) patterns were also measured for the zone-refined and 32-year-old materials. The extent of the Bragg peaks showed that amorphization of the 32-year-old sample had not occurred despite the prolonged exposure to self-radiation. Analogous to metastable δ -Pu alloys, the local atomic structure around Pu for the zone-refined material shows the possible presence of noncrystallographic Pu-Pu distances. Conversely, the Ce and the 32-year-old sample show no evidence for such noncrystallographic distances. Disorder in the Pu local environment was found to be impurity dependent. The Ce-doped sample presented a larger Pu-Pu nearest neighbor disorder than the aged sample, although the total amount of Am, U, and He impurities was actually higher in the aged sample. The local environment around U and Ce impurities is consistent with these elements being in substitutional lattice sites. In addition, U and Ce do not introduce significant lattice distortion to their nearest neighbors. This is consistent with disorder being more related to the perturbation of the coupling between the electronic and crystal structure, or the Peierls–Jahn–Teller distortion that generates the monoclinic α -Pu structure, and less to strain fields produced in the vicinity of the impurities.

DOI: 10.1103/PhysRevB.63.174111

PACS number(s): 61.10.Ht, 61.82.Bg, 61.80.-x

I. INTRODUCTION

Among other properties, the structural diversity of Pu is unique among the elements. At ambient pressure Pu transforms into a succession of six crystallographic phases between room temperature and its melting point at 914 K. In addition, these transformations are accompanied by large, nonmonotonic volume changes, with a 25% difference between the cubic (fcc) δ phase and the monoclinic α phase.¹ The low-temperature α phase is highly unusual because it is a metal with an open low-symmetry (monoclinic) crystal structure. It is also the densest form of Pu. Mechanically it is a hard, brittle metal that is nevertheless soft vibrationally, with a Debye temperature of ~ 200 K.² The origin of these structural (and other) properties of Pu has generally been attributed to the fact that it marks the boundary between the itinerant and the localized $5f$ electron systems. From Th through Np, the atomic volume displays the parabolic decrease typical of transition metals as the number of bonding electrons increases. However, the volume of the actinides jumps up sharply from Np to Am, ascribed to the localization of the $5f$ electrons.³ Pu is in the middle of this discontinuity, with α Pu slightly and δ Pu significantly above the trend through Np.

The explanation for the atomic volumes and the low symmetry structure of α -Pu has been a long-standing challenge for electronic structure methods. It is currently a testing ground for these methods due to the high directionality and the large density of states involved in f electron bonding.⁴ Among explanations for the structure of α -Pu, recently, *ab initio* relativistic total energy calculations have explained the crystal structure of α -Pu in terms of a Peierls–Jahn–Teller–

like distortion.⁵ This distortion splits a large $5f$ density of states (DOS) that crosses the Fermi energy in a higher symmetry cell. Thus, the total energy is minimized by lowering the symmetry of the crystal, resulting in the monoclinic α phase.⁶

Conventional crystallographic methods solve α -Pu as a monoclinic structure with 16 atoms per unit cell, space group $P21/m$, with eight unique atoms. All the atoms are located at either $(x, 1/4, z)$ or $(-x, 3/4, -z)$ positions. Six of the eight unique Pu atoms form four short bonds in the range 2.57–2.78 Å and ten long bonds in the range 3.19–3.71 Å. The seventh Pu atom forms five short and seven long bonds and the eighth unique atom forms three short and thirteen long bonds.⁷ Although the directionality of the $5f$ orbitals suggests bonds with covalent character and electronic localization as the origin of the local asymmetry, calculations instead find the Peierls–Jahn–Teller–like distortion. The identification of nanometer-scale heterogeneity or phase separation in metastable δ -Pu alloys together with the structural complexity of the α phase suggests that α -Pu is a good candidate for local deviations from the average structure.⁸ It is therefore of interest to determine if similar collective lattice distortions occur in the α phase, implying that they are intrinsic to Pu, or whether they only occur in and are specific to δ alloys. It is also of interest to determine if dopants have effects on the local structure of α -Pu analogous to those in the δ alloys.

The effects of trace elements, i.e., those occurring at concentrations well under one atom per unit cell, also raise the more general issues of the coupling of the induced local strain fields and disruption of the band structure around these defect sites to the solubility of the dopant element and its effects on the phase stability and other properties of the host.

Certain trivalent and tetravalent impurities (and divalent Zn) retain the δ phase at room temperature by an unknown mechanism.⁹ The measurement of lattice relaxations and the induced disorder on the average structure could lead to a better understanding of the microscopic origin of this δ stabilization mechanism. In addition, self-irradiation is an issue more specific to Pu and other actinides that will affect the structure via energy deposition and the introduction of non-Pu decay products. Self-irradiation in δ alloys has been found not only not to cause amorphization but also to promote the formation of the homogeneous stable δ local structure from the heterogeneous metastable one.⁸ The question then, is whether aging in α -Pu would amorphize the structure or, as in δ -Pu, it results in self-annealing and the preservation of long- and short-range order. As a complement to the average, long-range structure of the coherent fraction of a sample determined by conventional crystallographic methods, local structure measurements, e.g., x-ray absorption fine structure (XAFS) spectroscopy and x-ray-neutron pair distribution function analysis (PDF), are recognized as the best means of identifying and characterizing the local lattice distortions that are symptomatic of these kinds of localized and cooperative phenomena. XAFS also provides element-specific information on defect environments. This paper describes the results of synchrotron x-ray measurements on newly prepared (zone refined), new 0.34 at. % Ce-doped, and 32-year-old (with ~ 800 ppm U, ~ 1200 ppm He, ~ 3300 ppm Am as principal impurities) samples of α -Pu.¹⁰

II. EXPERIMENTAL PROCEDURE

Newly prepared α -Pu samples were purified by zone-refining, using a levitated molten zone to minimize the introduction of impurities. The temperature of the molten zone was 750 °C, and the atmosphere was 10^{-5} Pa. A total of ten zone refining passes were made at a travel rate of 1.5 cm/h. The total impurity concentration, excluding N, O, F, Cl, and Br, in the cleanest portion of the Pu specimen was 130 ppm. Uranium contributes 110 ppm. A complete description of this procedure is published elsewhere.¹¹ An aged sample slab was obtained from 32-year-old α -Pu stored at room temperature. Finally the 0.34 at. % Ce sample was prepared by adding 0.2 wt. % of high purity elemental Ce. Slices of the α samples were cut from the bulk pieces with a slow speed diamond saw using an environmentally safe Freon substitute as a coolant (RF-5070). The samples were then ground on both flat surfaces from 300 through 600 grinding paper and PF-5070. The samples were then hand polished initially with six and finally with one diamond abrasive using a mineral base lubricant. The samples were finally polished in an electrolyte composed of 10% nitric acid and 90% dimethylformamide, at a voltage of approximately 20 V dc with a stainless steel cathode. The samples were cleaned after the grinding step and after each mechanical polishing with PF-5070. After the electro-polish, they were thoroughly cleaned with ethanol and gently blown dry air.

X-ray diffraction (XRD) measurements were performed at the Stanford Synchrotron Radiation Laboratory (SSRL) beamline 7-2. The zone refined sample was measured at

room temperature while the 32-year-old sample was measured at ~ 100 K. The x-ray beam was set to 31 KeV to reduce the background from three Kapton windows of the containment system and to increase the penetration depth. A Ge detector coupled with a digital multichannel analyzer was used to select the elastic and the Compton inelastic component of the scattered beam. Rietveld refinement of the diffraction pattern was performed from $Q = 1.5$ to 8 \AA^{-1} where $Q = 4\pi \sin(\Theta)/\lambda$ (Θ being the diffraction angle and λ the x-ray wavelength), using the general structure analysis system (GSAS) Rietveld software.¹² Pair distribution function (PDF) analyses of these data from the Fourier transform of the diffraction spectra were inconclusive and not included. XAFS measurements were performed at beamline 4-2 of SSRL across the L_{III} absorption edge of Pu, and the Ce K and the U L_{III} edges of the appropriate samples. The XAFS data were analyzed up to $k = 13\text{--}15 \text{ \AA}^{-1}$ above the absorption edge, where k is the photoelectron wave number as defined below. Si(220) crystals were used to monochromatize the x-ray beam. Harmonic rejection was accomplished by tilting a flat Rh- or Pt-coated mirror to a cutoff energy of ~ 20 keV for the Pu and U edges. Due to the characteristic cutoff energy intrinsic of SSRL beamline 4-2, there is no need for harmonic rejection at the Ce K edge XAFS. The data were taken in fluorescence mode using a multielement Ge detector because the 100–250-micron-thick samples are opaque to the beam. The proper energy windows were set to obtain the fluorescence signal for the target element. The signal from 10–13 elements was averaged to obtain a scan in fluorescence mode. The reduction of the XAFS data was performed following standard procedures.¹³ Energy calibration was accomplished by defining the first inflection point of the K edge of a Zr foil as 17.99835 keV for the U and Pu edges. The Ce spectra were self-calibrated. The threshold free photoelectron energy E_0 was defined as 18.057 keV (the inflection point at the Pu L_{III} edge) such that the photoelectron wave number is $k = \sqrt{(2m/\hbar^2)(E - E_0)}$. The data were normalized by offsetting the spectra so that the value of a second order polynomial fit over the pre-edge was equal to zero and scaling the spectra so that the value of a third order polynomial fit over the region above the edge was equal to unity. The EXAFS $\chi(k)$ were extracted from the spectra as the difference between the normalized spectra and an adjustable spline function that approximates the smooth atomic portion of the absorbance. The parameters of this spline function were determined by minimizing the low frequency residuals ($R < 1.8 \text{ \AA}$) in the Fourier transform of each absorption spectra. The self-absorbance (for Pu) correction was introduced during the EXAFS extraction by dividing the difference between the data and spline by 0.39.¹⁴ Metrical parameters and subsequent radial distribution functions (RDF) were obtained by conventional, nonlinear least squares curve fits as described below, using amplitudes and phases calculated using the *ab initio* multiple scattering code FEFF.¹⁵ Curve-fits were performed on $\chi(k)$, the results are presented as $\chi(R)$ for ease in interpretation in terms of the actual structure.

TABLE I. Crystallographic structural parameters of the zone refined α -Pu sample derived from Rietveld refinement of x-ray diffraction data. The space group is $P2_1/m$ with all atoms at $(x, 1/4, z)$ sites. Lattice parameters are $a = 6.18595(32)$, $b = 4.82598(23)$, $c = 10.9719(6)$, and $\beta = 101.787(5)$. Thermal parameters U_{ISO} were constrained to be the same for all the sites with a value of $U_{\text{ISO}} = 0.41(5)$. The cell volume was found to be $320.639(30)\text{\AA}^3$. Units for cell constants are \AA and degrees, and for thermal factor 100\AA^2 .

Atom	x	y	z
Pu1	0.3390(11)	0.25	0.1565(7)
Pu2	0.7704(13)	0.25	0.1717(6)
Pu3	0.1345(12)	0.25	0.3406(7)
Pu4	0.6605(13)	0.25	0.4569(8)
Pu5	0.0314(11)	0.25	0.6210(7)
Pu6	0.4719(11)	0.25	0.6503(6)
Pu7	0.3275(12)	0.25	0.9302(7)
Pu8	0.8707(11)	0.25	0.8958(6)

III. RESULTS AND DISCUSSION

A. XRD

The diffraction pattern for the zone-refined sample was refined in terms of the α -Pu monoclinic structure reported by Zachariassen.⁷ Cell parameters and atom coordinates were left as floating parameters. The isotropic displacement parameter (U_{iso}) of all the atoms was constrained to be the same for all lattice sites to avoid correlation. The results of the refinement and a plot of the data and refinement are shown in Table I and Fig. 1(a), respectively. Cell parameters and atom coordinates were found to be in agreement with previous reports with the volume of the unit cell being ~ 0.2 and 0.6% larger than the volumes reported in Refs. 7 and 16. The isotropic thermal factor was found to be in agreement with the Debye temperature reported by Lawson (see Table I).²

For the 32-year-old sample, we have to take into account that Pu is constantly irradiating itself. The U recoil nucleus from the decay of Pu^{239} that constitutes $>90\%$ of typical Pu carries an energy of approximately 85 keV and converts nearly three quarters of this kinetic energy into atomic displacements before it comes to rest.⁹ Some workers in the field propose that because of the very high and rapid energy deposition the atoms along the recoil track are best considered as transiently molten. In typical Pu, it is estimated that every atom will have been shifted from its original position in the lattice within ten years. It is of obvious interest to know if the accumulated radiation damage will produce Frenkel pairs and other defects that eventually amorphize the sample—typical of most materials—or if there are other compensating mechanisms in Pu that will conserve its crystallinity and long-range order. For the 32-year-old sample, the narrow, large amplitude diffraction peaks past $Q = 7\text{\AA}^{-1}$ and the absence of a distinct diffuse background in the diffraction demonstrate that this sample is highly crystalline with no evidence of a significant amorphous component [see Fig. 1(b)]. This indicates that self-annealing mechanisms are very effective for Pu at ambient temperature.

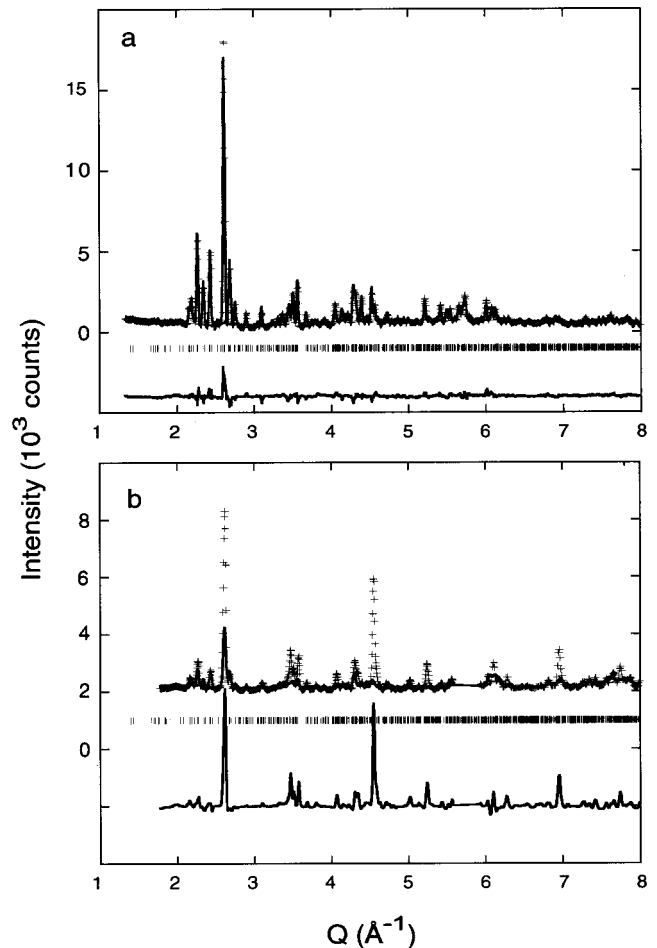


FIG. 1. X-ray powder diffraction data for (a) zone-refined α -Pu and (b) 32-year-old α -Pu. The plus (+) marks represent data while the continuous line is the calculated profile from Rietveld refinement. The tick marks indicate the positions of the allowed reflections in the monoclinic $P2_1/m$ space group. The lower curve indicates the difference between the observed and calculated profiles.

Additional information is provided by a more complete analysis. The refinement of the diffraction pattern from the 32-year-old sample based on the α -Pu structure demonstrates that, with a few exceptions, the measured pattern is that of the α phase. However, despite the basic similarities, there are evident differences that can be separated into two sets. A relatively small number of peaks are higher than the refinement by up to 200% of the amplitude, while a larger set of peaks differ from the refinement by ± 20 –50%. For the first set with the large errors, analysis of peak positions and related plane spacing and lattice parameters indicates that these peaks are not Al, Cu, or PuO_2 . This rules out the sample holder (made of Al and Cu) or surface corrosion as their source. Also, these Bragg peaks do not correspond to δ -Pu. This finding might imply the presence of an unknown Pu phase or compound, but if so its fraction is $<2\%$. The second set of smaller discrepancies could be more related to unidentified distortions of the α structure. Because of these discrepancies between the aged sample and the refinement, no attempt was made to obtain accurate atom positions. The

lattice parameters of the 32-year-old sample were found to be $a = 6.171(4) \text{ \AA}$, $b = 4.821(4) \text{ \AA}$, $c = 10.994(6) \text{ \AA}$, and $\beta = 101.80(5) \text{ \AA}$ with a cell volume of $320.1(4) \text{ \AA}^3$. The isotropic thermal factor was found to be $U_{\text{ISO}} = 0.006(1) \text{ \AA}^2$. The refinement, scaling cell volumes due to differences in measuring temperatures indicates no swelling of the lattice within the given uncertainties. The refinement of the 32-year-old sample also shows an increase in the isotropic thermal factor with respect to the zone-refined sample. These differences imply structural damage that may be not only from displacements resulting from ballistic conditions but also from the internal pressure induced locally by Am and trapped \AA scale He bubbles. Based on the minimal change in the cell parameters these types of defects appear to have little or negligible effect on the density on this decades time scale. Of course, all interpretations are subject to the caveat that diffraction and absorption data are lacking on this sample in its original state. In summary, self-radiation effects in Pu appear to slowly disorder the α -Pu structure while preserving the long-range order. The former conclusion is corroborated by the XAFS results discussed below.

B. Pu XAFS

The determination from XAFS of differences in local structure in complicated structures such as this begins with comparisons of Fourier transform of the XAFS $\chi(R)$. $\chi(R)$ is distorted relative to the actual element specific radial distribution function (RDF) by the phase shift of the modulus to lower positions and also by interference effects that often actually increase the sensitivity of $\chi(R)$ to small differences in the RDF. The Pu $\chi(R)$ of the zone-refined 32-year-old and 0.34 at. % Ce samples were obtained by Fourier transformation of the XAFS data over the region $3.4 < k < 12.8 \text{ \AA}^{-1}$. Additionally, as a guide in the description of the local structure, a calculation of $\chi(k)$ using the *ab initio* multiple-scattering code FEFF was done based on the reported crystal structure at 80 K.¹² This program has proven useful in calculating x-ray absorption cross sections in actinides.¹⁷ A configurational average of the XAFS simulations from the eight unique atoms in the structure was performed to include effects due to different local environments for each unique Pu atom in the unit cell. The simulation was then Fourier transformed and treated in the same way as the experimental data. This simulation shows that the first peak in $\chi(R)$ at $R - \Delta \sim 2.5 \text{ \AA}$ corresponds to Pu-Pu distances in the range $2.58\text{--}2.78 \text{ \AA}$ (short bonds) and the second peak at $R - \Delta \sim 3.5 \text{ \AA}$ corresponds to Pu-Pu distances between $3.2\text{--}3.72 \text{ \AA}$ (long bonds). Here, Δ represents the phase shift of the photoelectron that produces peaks in the Fourier transform of the XAFS data that are $\sim 0.1 \text{ \AA}$ shorter than the actual bond length for Pu-Pu. An overlay of the simulation and the XAFS $\chi(R)$ data is shown in Fig. 2. The simulation follows the major features of the data, however we observe a small shift towards lower distances for the second peak corresponding to the contributions from the longer set of first shell Pu-Pu distances and significantly higher amplitudes and shifted peak positions at large R . The differences in amplitude could be related to disorder or to the simplifications assumed in

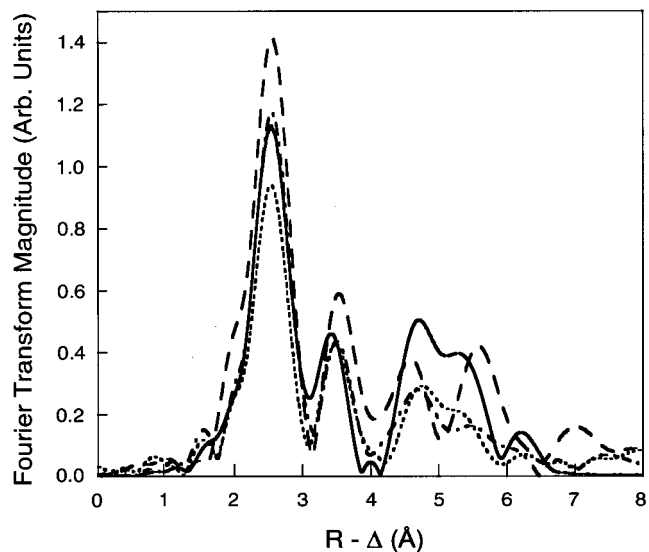


FIG. 2. Fourier transform magnitude of the XAFS from the calculated profile based on crystallographic data (solid line), the unged zone-refined sample (dashed line), the 32-year-old sample (dot-dashed line), and the Ce-doped sample (dotted line).

using the correlated Debye model for the Debye-Waller factor, while differences in peak positions could be the result of accumulated displacements and distortions that become more pronounced for more distant shells. Also, the differences in peak positions are difficult to evaluate qualitatively because the large number of neighbor atoms included in each peak.

The experimental data not only show differences relative to the simulation but also with respect to each other in the amplitude of the largest peak at $R - \Delta \sim 2.4 \text{ \AA}$. The zone refined sample displays the highest peak, higher even than the calculation, while the aged sample has a very similar amplitude to the calculation and the Ce sample is significantly lower. Diminished amplitude has to be correlated with increased disorder, if the reasonable assumption is made that the number of nearest neighbors is conserved. Based on calculations of the decay products with time,¹³ the 32-year-old sample contains about 0.33 at. % Am, 0.12 at. % He, and 0.08 at. % U as its principal impurities. The total impurity concentration in the aged sample is thus larger than the amount of Ce in the doped sample, implying that Ce is more efficient than the decay products in disrupting the crystalline structure of α -Pu, at least for these nearest neighbors. Higher peaks in $\chi(R)$ also show differences. The amplitude for the zone refined sample remains higher than all of the spectra through the more distant Pu first shell peak, and higher than the other samples but not the calculation through $R = 6 \text{ \AA}$. This spectrum also displays shifts in the peak positions and overall pattern relative to the others at the longer distances. Although the amplitude of the calculation for the more distant first shell peak is similar to the aged and 0.34 at. % spectra, it is shifted somewhat to lower R , implying more weight towards lower distances in its atom distribution. Although the interpretation of these changes at this qualitative level of analysis is obscured by the fact that the static distributions of these shells are already wide and somewhat sensitive to even small changes in the disorder, it can neverthe-

less be safely assumed that lower amplitudes continue to reflect wider and/or less harmonic distributions.

Quantitative information about the Pu neighbor environment for the elucidation of these results is obtained from curve fits to the XAFS. Due to the fact that it is not possible to fit all the Pu-Pu shells of the α -Pu $\chi(R)$ because of parameter correlation,¹⁸ we used a simplified approach for fitting and extracting information from the data. We first performed a fit of the XAFS simulation over the range $k=3.4 < k < 12.8 \text{ \AA}^{-1}$ and $R=2.5\text{--}6.0 \text{ \AA}$ using the standard XAFS equation¹⁴ and identifying the minimum number of neighbor shells to give an adequate fit. To further reduce the number of free parameters for the required eight shells and to avoid parameter correlation we fixed additional parameters. We chose to fix σ and left N floating based on the observed instability of σ during trial fits. A reason for this could be that we are using a single Gaussian peak to represent a number of closely spaced Pu-Pu distances that do not necessarily follow a Gaussian distribution. ΔE_0 was fixed at the same value for all shells based on averaging the results from fits in which this parameter was unconstrained. This scheme provided the best way for extracting information from the data. In addition, rather than interpret the RDF's from the metrical results of the curve fits, we performed direct comparisons of the resulting RDF's, a strategy that we have used successfully before.¹⁹ The optimum approach derived from this method was a fit using two shells for short nearest neighbor Pu-Pu distances, two shells for the longer nearest neighbor distances, and then four more shells through 6 \AA . This not only gives reasonable fits but also adequately models the actual PDF.

After these details of the method were developed from theoretical spectrum, we fit the experimental spectra identically using the values from the calculated spectrum as starting points. A plot of the fits is shown in Fig. 3 and the numerical results are shown in Table II. For the short-bonds we observe (Fig. 4) that the second Gaussian which represents the longer portion of the short bonds decreases substantially in amplitude between the zone-refined and the 32-year-old sample while the first Gaussian, which represents the shortest portion remains basically constant. If the number of atoms remains constant then these changes most likely actually reflect an asymmetric broadening of the Pu distribution on the high R side of this cluster of distances. Between the 32-year-old and the 0.34 at. % Ce sample a decrease in amplitude is observed also for the first Gaussian, in agreement with our qualitative description which showed a strong effect of Ce dopants in the short-bonds region and implies a broadening of the distribution, albeit a smaller one, in this region too. The third and fourth Gaussians, representing the long bonds of the Pu first shell, decrease concomitantly in amplitude while also preserving their relative amplitudes, probably reflecting an overall broadening and greater tendency towards asymmetry in this set of Pu-Pu pairs. The fifth Gaussian at $4.3\text{--}4.5 \text{ \AA}$, shows a trend towards higher R as well. However, the RDF shows that in this region there is no stable minimum for the single Gaussian and thus the observed trends do not necessarily represent any real phenomena, despite the fact that the crystallographic RDF shows

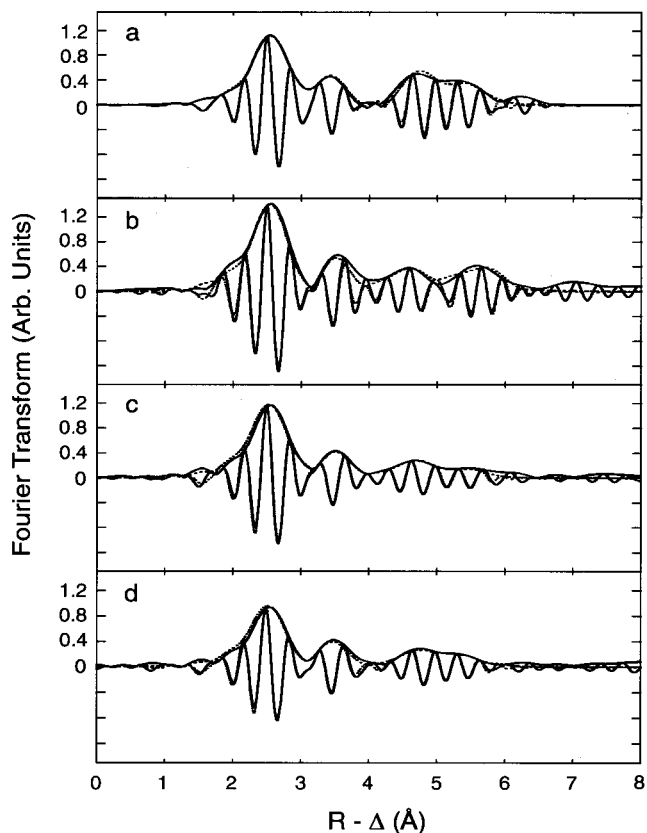


FIG. 3. Fourier transform of the data (solid line) and fit (dotted line) for the calculation based on crystallographic data (a), unaged zone refined sample (b), 32-year-old sample (c), and Ce-doped sample (d). The oscillations are the real part and the envelope represents the magnitude of the Fourier transform.

substantial, separated atomic density in this region. Finally, the greater long range order in the zone-refined sample with the smallest number of defects is reflected in the very large amplitudes of the shells beyond 5 \AA .

The simplified approach to extract information from the data enhanced the similarities between samples by reducing the number of parameters. However, the possibility still remains that there are local distortions that are reflected in Pu-Pu pairs outside of these standard α distances. Such distortions are suggested by the differences between the data and the fits (Fig. 5). Whereas the correspondence between the data and the fit is excellent over the full range for the spectrum of the aged sample and displays only small differences in the second, third, or fourth shell region for the calculation, small but significant differences are observed for the 0.34 at. % Ce and especially for the zone refined spectrum. To investigate these differences between the samples we analyzed the difference between the data and fit for each spectrum (Fig. 5). For the zone-refined sample [Fig. 5(b)] we observe two peaks at $R - \Delta \sim 2.8$ and 3.5 \AA that are 10–20% as large in amplitude as the total spectrum in those regions. These could indicate Pu-Pu distances in a region that is crystallographically forbidden, i.e., between the short- and long-bond regions. A fit to these features with Pu shells fits the real part quite well and does reflect the pattern in the modu-

TABLE II. Results of the fits to the XAFS indicating the distance (R), scale factor (N), and Debye-Waller factor (σ) for the Pu-Pu short and long bonds and the U-Pu and Ce-Pu average distance. See text for details of the fitting procedure.

	Pu-Pu in calculation	Pu-Pu in zone refined	Pu-Pu in 32-year-old	U-Pu in 32-year-old	Pu-Pu in 0.34 at. % Ce	Ce-Pu in 0.34 at. % Ce
R	2.57(1)	2.59(1)	2.61(1)	2.64(3)	2.60(1)	2.61(3)
N	1.5(5)	3.0(6)	2.8(6)	3.7(1.0)	2.5(6)	2.8(0.8)
σ	0.05	0.05	0.05	0.01	0.05	0.1
R	2.67(1)	2.69(1)	2.72(1)		2.71(1)	
N	2.2(5)	2.6(3)	1.1(3)		1.1(3)	
σ	0.05	0.05	0.05		0.05	
R	3.29(1)	3.27(1)	3.29(1)		3.27(1)	
N	3.1(8)	4.8(8)	4.2(8)		2.8(8)	
σ	0.06	0.06	0.06		0.06	
R	3.44(1)	3.44(1)	3.45(1)		3.43(1)	
N	4.7(1.0)	6.6(1.2)	5.2(1.2)		4.4(1.2)	
σ	0.06	0.06	0.06		0.06	

lus, indicating the possibility of Pu-Pu distances at $\sim 3.02(2)$ and $3.27(2)$ Å. The feature at 3.27 Å falls within the region of long bonds. However the feature at 3.02 is in the forbidden region. To obtain a reasonable fit it was required to

increase the Debye-Waller factor to ~ 0.15 , which indicates a broader or disordered distribution of Pu-Pu distances around the mean. Putting these extra shells back into the original fit does improve their quality in these regions but renders them

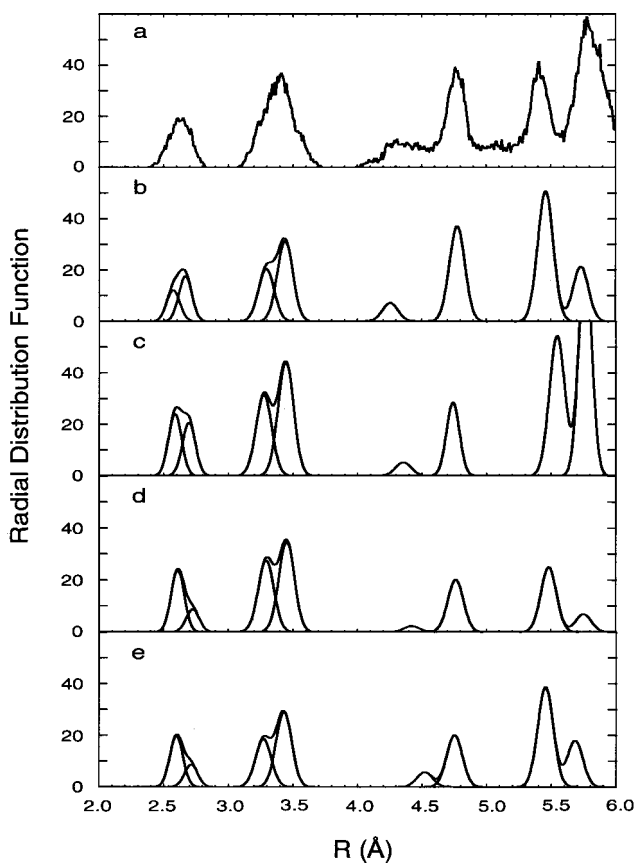


FIG. 4. Radial distribution function of α -Pu from crystallographic data (a), and radial distribution function from fits to the XAFS for the calculation (b), zone-refined sample (c), 32-year-old sample (d), and Ce-doped sample (e).

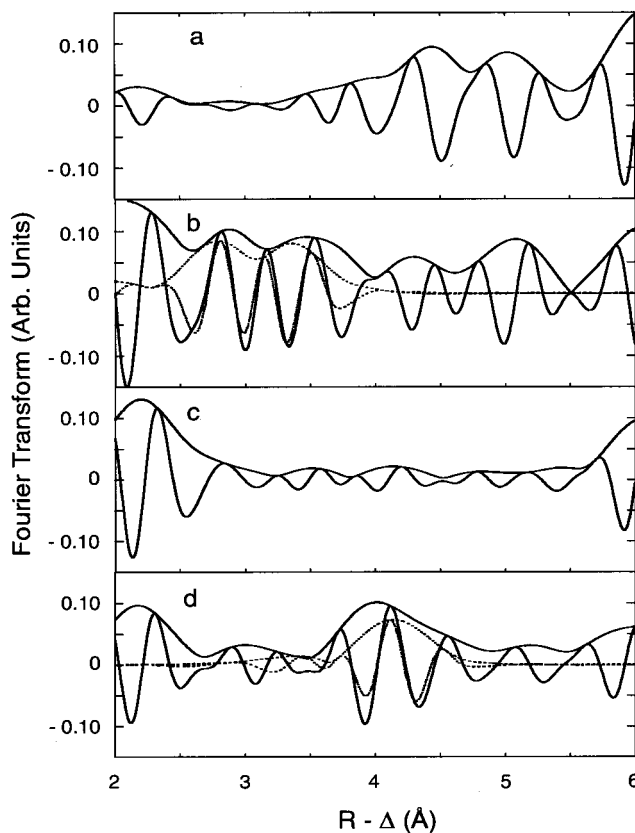


FIG. 5. Fourier transform magnitude of the difference between the XAFS and fit for the calculation based on crystallographic data (a), zone-refined sample (b), 32-year-old (c), and Ce-doped sample (d). The oscillations are the real part and the envelope represents the magnitude of the Fourier transform. Fits (dotted line) are presented for the zone-refined and Ce-doped samples.

less stable because of overdetermination. Although the lower amplitudes render these results less certain than those pertaining to the crystallographic structure, there is nevertheless a distinct possibility that there are local distortions in this sample. For the 32-year-old sample [Fig. 5(c)] no relevant features are observed in the difference between the XAFS data and fit. For the Ce-doped sample, a feature around $R - \Delta \sim 4.0 \text{ \AA}$ is observed. A fit to that feature with a single Pu shell provided a Pu-Pu distance 4.24 \AA . This distance falls within the region at the left of the fifth Gaussian in the radial distribution function [Fig. 4(e)] and may therefore simply reflect a lower degree of ordering in the $4.2\text{--}4.5 \text{ \AA}$ region rather than a distortion from the crystal structure. Returning to the anomalous peak in the zone-refined sample, we note that a similar and intriguing behavior has been observed in metastable δ -Pu alloys. In unaged, metastable δ -Pu alloys a deviation from the δ fcc structure has been reported in samples with concentrations of δ stabilizers that place them in proximity to the α - δ boundary. The most striking feature is that this anomaly disappears with aging and with higher trace element concentrations.⁸ Whether or not we are observing a similar behavior cannot be answered by this study because of the diminished level of certainty associated with these results on a fundamentally more complicated material.

C. U and Ce XAFS

In this study, what is perhaps the most remarkable finding is the substantial effect on the average local structure around Pu resulting from the substitution of 1 Pu atom out of around 300 by Ce, which is also the case for the decay products Am, U, and He. A starting point in understanding this is the determination of whether these impurities substitute for Pu in the lattice or not and how they strain the lattice locally. A useful construct for modeling the effects of the impurity atom could be that of a strain field as a map of the local order parameter, whose magnitude is given by the extent of the displacement of a neighboring atom from its lattice position. Although in most cases it is likely that the field amplitude decreases monotonically with distance from the defect, recent calculations on Martensitic systems near the transformation point indicate that the interaction of the local field and the longer range strain can have complex and far reaching consequences on the structure.²⁰ Another possibility for inducing far-reaching small atom displacements or disorder by this relatively small quantity of impurities is the effect on the electronic structure that could be produced. Since the formation of the monoclinic α structure has been related to a Peierls–Jahn-Teller–like distortion via the very narrow f -band crossing the Fermi level, then it could be the case that Ce and other impurities would have a disproportionately large effect on the distortion, and thus on the α -Pu structure.

The results of the fits of the XAFS from U and Ce are shown in Fig. 6 and Table II. We note that because of the high noise levels resulting from the low solute concentrations, we only attempted to determine the shortest U-Pu and Ce-Pu distances. This would determine whether the trace atom was substituting into the α lattice directly and, if so, whether there was a local strain associated with it. The re-

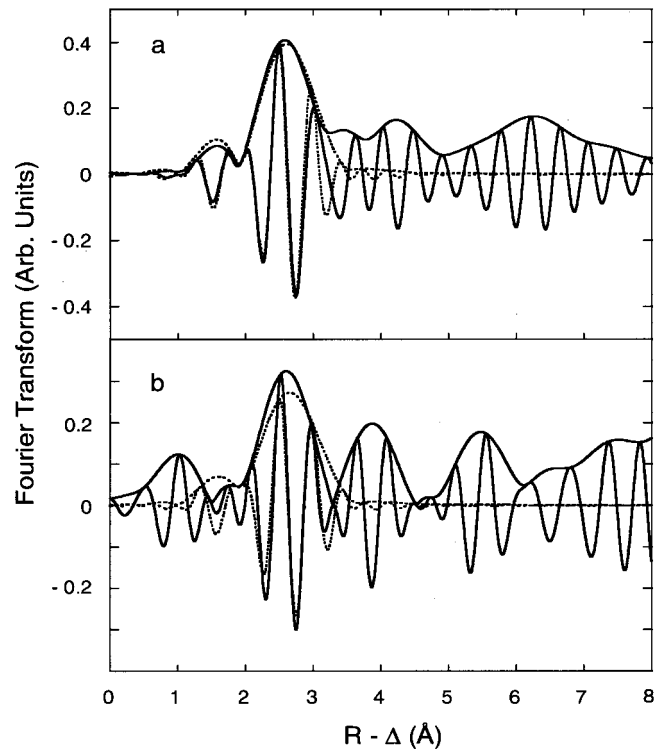


FIG. 6. Fourier transform of the XAFS data (solid line) and fit (dotted line) for (a) Ce impurities in the Ce-doped sample and (b) U impurities in the 32-year-old sample.

ported distance represents the average (U/Ce)-Pu distance for the nearest neighbors. For both U and Ce, the (U/Ce)-Pu distance found by the curve fits is in agreement with the Pu-Pu average for the short bonds within the uncertainty level of 0.03 \AA . For U, the results of the fits are consistent with its small volume and propensity for high density structures, although the 0.13 \AA contraction of the U-Pu bond length relative to the shortest U-U bond length in orthorhombic U implies that the U is either somewhat compressed or that its electronic orbitals have been modified relative to that in pure U. A much larger contraction relative to the pure element is found for the Ce, whose 2.61 \AA Ce-Pu bond length represents a 23% contraction from the Ce-Ce distance even of the high pressure α phase of pure Ce. Both atoms conform to the α -Pu lattice, displaying no signs of imposing significant elastic strain on the host Pu, which would be expected to be evinced most strongly in the nearest neighbor distances. The contraction of these trace elements from their native sizes and their effects on the total structure out of proportion with their relative amount implies a substantial influence of the impurities on the coupling between the electronic and crystal structure of the native metal.

IV. CONCLUSIONS

The results from XRD for the zone-refined sample showed agreement with the reported crystallographic structure and thermal factors. For the 32-year-old sample XRD showed that the sample retained excellent crystallinity. This

is notable since, due to the α decay process, each atom in the structure has been shifted from its position at least 3 times. However, a portion of the XRD pattern was not consistent with only the α structure. Possible explanations could include the presence of non-Gaussian distributions and/or unidentified impurity phases. The fits to the XAFS showed general agreement with the crystallographic structure. However an analysis of the residuals, or the difference between the data and fit provided evidence for an anomalous Pu-Pu distance between the short and long bonds region for the new zone-refined sample. Unfortunately the relative weakness of the signal does not allow a definitive identification of its presence. For the 32-year-old and the Ce doped samples XAFS measurements showed no Pu-Pu distances in crystallographic forbidden regions, i.e., between the short and long bonds and in the region after the long bonds [see Fig. 4(a)]. Also, U as a decay product of Pu was found to be consistent with a substitutional impurity with a U-Pu nearest neighbors distance in agreement with the Pu-Pu short bonds. The measured XAFS Ce-Pu distance was found also to be consistent with the average Pu-Pu short and long bonds. The small amount of Ce atoms with respect to Pu atoms and the lack of

evidence for strain-induced disorder thus indicates that disorder in the structure could be more related to the effects of the impurities on the coupling between the electronic and crystal structure rather than impurity induced localized strain fields. In terms of the general issue of trace elements in hosts, the enormous contraction of the Ce atom in the α -Pu lattice and the implied effect of the α -Pu on the Ce electron structure are quite notable.

ACKNOWLEDGMENTS

F.J.E. wishes to thank A. C. Lawson for his invaluable advice and S.S. Hecker for his comments and insights. XRD and XAFS experiments were performed at the Stanford Synchrotron Radiation Laboratory, which is operated by the U.S. Department of Energy, Office of Basic Energy Sciences. The experimental measurements and analysis of the data were supported by DOE Defense Programs and the interpretation and modeling were supported by DOE/OBES Division of Chemical Sciences under Contract No. W-7405. Health operations at SSRL were supported by the Seaborg Institute for Transactinium Science at LANL.

-
- ¹W. N. Miller and F. W. Schonfeld, in *Plutonium Handbook, a Guide to Technology*, edited by O. J. Wick (The American Nuclear Society, La Grange Park, Illinois, 1980), Vol. 1, p. 31.
- ²A. C. Lawson, B. Martinez, J. A. Roberts, B. I. Bennet, and J. W. Richardson, Jr., *Philos. Mag. B* **80**, 53 (2000).
- ³J. M. Wills and O. Eriksson, *Phys. Rev. B* **45**, 13 879 (1992).
- ⁴M. D. Jones, J. C. Boettger, R. C. Albers, and D. J. Singh, *Phys. Rev. B* **61**, 4644 (2000).
- ⁵P. Soderlind, J. M. Wills, and O. Eriksson, *Phys. Rev. B* **57**, 1320 (1998).
- ⁶P. Soderlind, J. M. Wills, B. Johansson, and O. Eriksson, *Phys. Rev. B* **55**, 1997 (1997).
- ⁷W. H. Zachariasen, *Acta Crystallogr.* **16**, 777 (1963).
- ⁸S. D. Conradson, *Appl. Spectrosc.* **52**, 252A (1999).
- ⁹S. S. Hecker and J. C. Martz (unpublished).
- ¹⁰W. G. Wolfer (unpublished).
- ¹¹J. C. Lashley, M. S. Blau, K. P. Staudhammer, and R. A. Pereyra, *J. Nucl. Mater.* **274**, 315 (1999).
- ¹²A. C. Larson and R. B. VonDreele (unpublished).
- ¹³P. A. Lee, P. H. Citrin, P. Eisenberger, and B. M. Kinkaid, *Rev. Mod. Phys.* **53**, 769 (1981).
- ¹⁴L. E. Cox, R. Martinez, J. H. Nickel, S. D. Conradson, and P. G. Allen, *Phys. Rev. B* **51**, 751 (1995).
- ¹⁵A. I. Ankudinov, B. Ravel, J. J. Rehr, and S. D. Conradson, *Phys. Rev. B* **58**, 7565 (1998).
- ¹⁶G. H. Kwei, D. Louca, S. J. L. Billinge, and H. D. Rosenfeld, in *Local Structure from Diffraction*, edited by S. J. L. Billinge and M. F. Thorpe (Plenum, New York, 1988), p. 323.
- ¹⁷A. I. Ankudinov, S. D. Conradson, J. Mustre de Leon, and J. J. Rehr, *Phys. Rev. B* **57**, 7518 (1998).
- ¹⁸The total number of independent points in the spectra is $N_{\text{ind}} = 2\Delta k\Delta R/\pi \sim 18$. *X-Ray Absorption Fine Structure Spectroscopy VI*, edited by S. Hasnain (Ellis and Horwood, Chichester, England, 1991).
- ¹⁹T. A. Tyson, J. M. de Leon, S. D. Conradson, A. R. Bishop, J. J. Neumayer, H. Roder, and J. Zang, *Phys. Rev. B* **53**, 13 985 (1996).
- ²⁰S. R. Shenoy, T. Lookman, A. Saxena, and A. R. Bishop, *Phys. Rev. B* **60**, 12 537 (1999).